International Communications in Heat and Mass Transfer 132 (2022) 105887

Contents lists available at ScienceDirect

International Communications in Heat and Mass Transfer

journal homepage: www.elsevier.com/locate/ichmt

Water production enhancement from the air moisture using nanofluids-experimental investigation and exergo-enviroeconomic analysis

Masoud Kaveh [a], Ali Heydari [b,*], Nader Rahbar [c], Abdollah Khalesi Doust [c]

[a] Department of Mechanical Engineering, Semnan Branch, Islamic Azad University, Semnan, Iran
[b] Department of Mechanical Engineering, University of Torbat Heydarieh, Torbat Heydarieh, Khorasan Razavi, Iran
[c] Energy and Sustainable Development Research Center, Semnan Branch, Islamic Azad University, Semnan, Iran

ARTICLE INFO

Keywords:
Water production
Air humidity
Refrigeration cycle
Nanofluid
Dew point

ABSTRACT

Nowadays, the expansion of communities and population growth has further highlighted the need for clean water. To solve this problem, various methods have been proposed. Water extraction from the air moisture is of these methods which involve cooling the air to its dew point in which the moisture transforms from the gas to the liquid phase. In the present study, a device consisting of a refrigeration cycle and a moisture distillation cycle was designed to provide pure water from the air moisture. Additionally, it was tried to enhance the system performance by dispersing nanoparticles such as Cu and Al_2O_3 into the working fluid of the heat exchanger. In this study, the influence of various parameters (including inlet air velocity and ambient humidity) on the performance of the system was investigated. Finally, an exergo-enviroeconomic analysis was performed in terms of water production and cost. Based on the results, with increasing the air humidity from 40% to 60%, the amount of water production of the system raised from 0.5 to 1.8 cc/min. It was also observed that dispersion of Cu and Al_2O_3 nanoparticles enhanced the water production by around 43% and 29%, respectively. Moreover, an increment in inlet air velocity reduced the water production; while increasing the air humidity had a constructive effect on the system performance. The economic analysis indicated that the water production during a year increased by about 42% upon using Cu nanofluid as the working fluid of the distillation cycle which declined the water production cost by 32%.

1. Introduction

Regarding the large population of communities and the limitation of water availability, many people do not have access to healthy sources of water. According to UN reports, about one-third of the world's population suffers from the shortage of drinkable water [1]. One of the best methods to provide pure water in different climate conditions is the extraction of water from air humidity through the moisture distillation cycle [2]. In this method, the temperature of the air is reduced below its dew point temperature, giving rise to phase transfer of the air humidity from gas to the liquid. First, there is a necessity to define a direct and indirect description of air humidity extraction system. If in a refrigeration cycle, the refrigerant directly cools the air in a heat exchanger (evaporator), this system is called direct water production from the air (DWPA). But if the refrigerant in the evaporator has cooled the intermediate fluid which transfer to a heat exchanger and cool the air, this system is called indirect water production from the air (IWPA). DWPA systems obviously have higher performance in compared with IWPA systems. But, in many systems, direct and indirect extraction water from the air moisture have their own advantages and disadvantages depend on the application of the system. For example, assume a system which water consumers are far from each other in a wide area. Using DWPA system individually for each consumer is very expensive and there is no economic justification. What is needed is the use of a central refrigeration system and water production nodes (heat exchangers) in the network. With large distances between the consumers and the central refrigeration system, using a compressor and sending refrigerant gas to heat exchangers is much more expensive than employing a pump and sending cooled liquid to heat exchangers. The purpose of examining IWPA systems should be to improve their performance.

Until now, some researchers have tried to produce water by different methods and the construction of various devices [3–5]. In an experimental study by Garg et al. [6], a solar cycle combined with a water desalination cycle was used to produce fresh water. In this study, the solar collector raises the water temperature and stores it in a tank.

* Corresponding author.
E-mail address: a.heydary@torbath.ac.ir (A. Heydari).

https://doi.org/10.1016/j.icheatmasstransfer.2022.105887

Available online 18 January 2022

Nomenclature

A	Heat transfer area (m^2)
$ACDE$	Annual carbon dioxide emission (kg/year)
AMC	Annual maintenance cost ($/year)
ASV	Annual salvage value ($/year)
C_p	Specific heat capacity ($J{\cdot}kg^{-1}{\cdot}K^{-1}$)
COP	Coefficient of performance
CPL	Cost of 1 Liter of produced water ($/year)
CRF	Capital recovery factor
D	Diameter of the fluid channel (m)
Ex	Exergy (J)
$\dot{E}$	Power (W)
E_{in}	Embodied energy (kWh)
$(E_{en})_{out}$	Annual output energy (kWh/year)
$(E_{ex})_{out}$	Annual output exergy (kWh/year)
EPBT	Energy payback time (year)
EPF	Energy production factor
FAC	First annual cost ($/year)
h	Enthalpy ($kJ{\cdot}kg^{-1}$)
I	Electrical current
i	Lending bank interest
k	Conductivity ($W{\cdot}m^{-1}{\cdot}K^{-1}$)
LCDE	Lifetime carbon dioxide emission (kg)
$\dot{m}$	Mass flow rate ($kg{\cdot}s^{-1}$)
M	Annual water production (L/year)
n	Lifetime of device
P	Pressure of fluid (Pa)
Ps	Goods price
$\dot{Q}$	Heat transfer rate (W)
R	Exergoeconomic parameter (kWh/$)
T	Temperature (K)
S	Salvage value ($)
SFF	Sinking fund factor
u	uncertainty
UAC	Uniform annual cost ($/year)
V	Voltage
W	Aperture wide (m)
$\dot{W}_{el}$	Electrical power (W)
X_{CO_2}	International price of carbon ($)
Z_{CO_2}	Price of the CO2 mitigation ($)

Greeks

$\phi_{en,\ CO_2}$	Environmental parameter ($tonCo_2$)
$\phi_{ex,\ CO_2}$	Exergoenvironmental parameters (ton Co_2)
μ	Dynamic viscosity of fluid ($kg{\cdot}m^{-1}{\cdot}s^{-1}$)
$\varnothing$	Mass fraction of nanofluid
η	Efficiency (%)
ρ	Density of material ($kg{\cdot}m^{-3}$)

Subscripts

air	Air
ave	Average
amb	Ambient
bf	Base fluid
c	Cold
comp	Compressor
con	Condenser
el	Electrical
en	Energy
ex	Exergy
eva	Evaporator
fluid	working fluid of the water distillation cycle
g	Glass cover
h	Hot
HE	1st heat exchanger
in	Inlet
loss	Loss energy
l	Produced fresh water
nf	nanofluid
out	Outlet
p	nanoparticle
r	Standard test condition
s	Solid
ST	Storage tank
SP	Spiral pipe
th	Thermal
v	Vapor
w	Wind

Afterward, the water in the desalination evaporates by the spraying process. Then, the evaporated water is directed to the condenser, resulting in fresh liquid water production. In another study conducted by Al-Enezi et al. [7], it was observed that reducing the flow rate of hot water enhanced the performance of the water desalination cycle. They also reported improved performance of the cycle by lowering the cold water temperature, increasing the hot water temperature, and raising the inlet air flow rate. Moreover, in a numerical study, Ibrahim et al. [8] investigated the amount of water production using a coupled solar system with an absorption chiller. In this study, the effect of various parameters such as fluid mass flow rate, fluid temperature, and air humidity was studied. Additionally, the performance of a water desalination cycle using solar energy and dehumidification processes was explored by Fouda et al. [9]. It should be noted that, in addition to using solar energy for freshwater production [10–12], some other researchers attempted to provide water by using some novel methods such as heat pumps [13–15] and thermoelectric modules [16–18].

The performance of a desalination water cycle using a heat pump was studied by Lawal et al. [15]. They addressed the effect of various parameters such as working fluid mass flow rate and airflow rate on the performance of the system. Besides, the effect of the thermoelectric module of the desalinated water was experimentally investigated by Al-Madhhachi and Min [19]. In this research, the cold and hot water flow in the cold and hot side of the thermoelectric module, respectively. Freshwater is produced by evaporating water in the hot side of the thermoelectric.

Also, Habeebullah [20] studied the performance of a refrigeration cycle in water production from air humidity. He observed that an increase in air velocity declined the water production of the system. Moreover, a reduction in the air velocity may lead to ice creation on the pipes of the system, which considerably declines the performance of the system. In another experimental study by Zolfagharkhani et al. [21], a gas refrigeration cycle was used to extract water from air humidity. They studied the effect of various parameters such as ambient temperature and humidity on the performance of the system and observed that the system can produce 24 L/day water.

In addition to selecting a suitable method for water production, the use of appropriate components and the efficient working fluid in the refrigeration and water distillation cycles can dramatically affect the performance of the system. In recent years, attention has been raised toward nanoparticles and their application in the engineering sciences [22,23]. The dispersion of nanoparticles in the base fluid can enhance the heat transfer coefficient of the fluid [24,25]. The shape, size, and material of nanoparticles are influential on the system performance

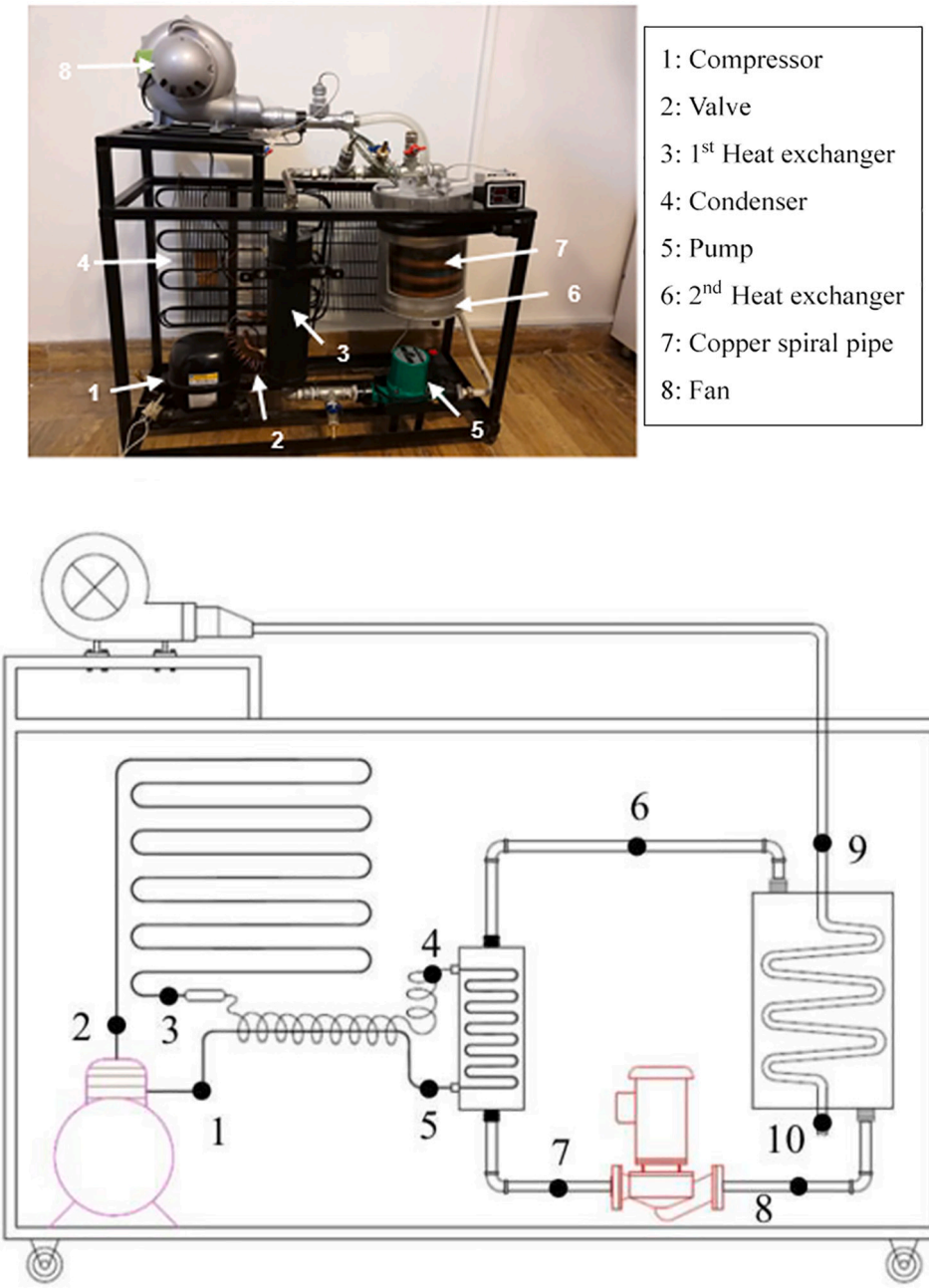

Fig. 1. The designed experimental setup.

[26]. In a numerical study, Garg et al. [27] investigated the performance of a coupled system consisting of a humidification–dehumidification desalination system and a nanofluid-based solar collector. In this study, the effect of various parameters including nanoparticle mass fraction and the diameter and length of the collector were studied.

The condensation process also depends on the geometry of the distillation heat exchanger. Investigation of R-404A fluid condensate inside a spiral pipe was addressed by Salimpour et al. [28] considering the effect of curvature and pipe diameter. It was observed that a decline in the pipe diameter enhanced the system performance. Essalhi et al. examined the performance of a helical coil condenser in the absorption refrigeration cycle with water and lithium working fluid [29]. They reported a decline in the volume and weight of the system by the spiral coil which improved the performance. Moreover, the performance of a copper condenser was evaluated by Liu et al. under various working conditions [30]. The effect of different parameters including inlet water temperature, inlet water velocity, and heat flux was studied. Moreover, condensation of R-134a fluid inside a flat, spiral tube and a spiral tube with a wavy inner surface was explored by Solanki and Kumar [31] who observed the best performance in the spiral tube with the inner surface of the wave.

According to the literature review, there is a significant gap for evaluation indirect water production from the air (IWPA). Therefore, in this study, the main goal is to improve the performance of a IWPA system and its economic analysis. Thus, it is attempted to produce water from the air moisture by coupling a refrigerant cycle and a water distillation cycle. In this study, the effects of various parameters including air velocity and ambient humidity on the performance of the system are evaluated. Moreover, the effect of dispersion of Cu and Al_2O_3 on the water production of the system is investigated. At the end of the research, an exergo-enviroeconomic analysis is carried out by comparing the water production, output energy and output exergy of

Table 1
The specifications of the experimental setup.

Specification	Value
Length of the spiral pipe	3 m
Diameter of the spiral pipe	2 cm
Capacity of the 2nd heat exchanger	5 litter
Compressor power	77 W
Fan power	110 W
Pump power	45 W

Table 2
Thermal properties of the Cu and Al_2O_3 nanoparticles.

Nanoparticle	Density (kg. m^{-3})	Heat capacity (J. $kg^{-1}.K^{-1}$)	Thermal conductivity (W. $m^{-1}.K^{-1}$)
Cu	8933	385	401
Al_2O_3	3970	765	40

nanofluid-based and water-based systems.

2. Experimental setup

In this study, the fabricated setup is consists of two different sections a refrigerant cycle and a water distillation cycle as illustrated in Fig. 1. The refrigerant cycle consisted of an AZ A1330YK-R compressor, an evaporator, an expansion valve, and a condenser. The water distillation cycle included 1st heat exchanger (as the evaporator of the refrigeration cycle), pump, and 2nd heat exchanger with a spiral coil. Note that the working fluids of the refrigerant cycle and water distillation cycle are R134a and pure water (or nanofluid), respectively. In this system, the refrigerant entered the compressor and exited with extremely high pressure. Then, in the condenser, the refrigerant releases its heat to the surrounding environment at a constant temperature and transfer from the gas to the liquid phase. By the passage of the refrigerant from the valve, the fluid absorbs the heat in the evaporator (heat exchanger) at constant pressure.

Moreover, in the second cycle, the base fluid (water or nanofluid) transfers its heat to the refrigerant in the heat exchanger. Afterward, the base fluid moves toward the pump and gains the needed energy for circulation in the cycle. After the passage of the base fluid from the pump, it enters the 2nd heat exchanger and absorbs the heat of the air flowing in the copper spiral pipe. Finally, the base fluid exits from the 2nd heat exchanger and enters the heat exchanger. As a result, in the current study, the fan blows the air from the ambient to the copper spiral pipe which releases its heat to the base fluid of the water distillation cycle. By reduction in the temperature of the airflow below the dew point, the moisture content of the air is transferred into the liquid water and released from the copper spiral pipe.

To analyze the performance of the system, the temperature of the working fluid of the water distillation cycle at the inlet and outlet of the 2nd heat exchanger was determined by a K-type thermocouple. Moreover, for determining the air humidity a Testo 605i thermohygrometer was employed. An anemometer (Terminator Termo Anemometer type: AVM-07) was utilized to measure the air velocity in a spiral pipe. The specifications of the components of the system are presented in Table 1.

2.1. Nanofluids specifications

As mentioned earlier, metal nanoparticles (NPs) (Cu and Al_2O_3) were dispersed in the working fluid (water) of the water distillation cycle to enhance the freshwater production of the system. The NPs properties are presented in Table 2. It should be noted that the mass fraction of the NPs was about 0.2%.

The mass flow rate of water and nanofluids are approximately the same. Since the volume fraction used for nanofluids is small, adding nanoparticles to water changes its density to a small extent. For example, for Cu nanoparticles, adding 0.2% Cu nanoparticles to water increases the density of water by 1.5% (Table 3), which has a negligible change. On the other hand, the pump used in the cooling fluid cycle has a constant rotating speed and the same volumetric flow rate in all tests (0.00387 lit/s). Therefore, it can be said that the mass flow rate of nanofluids and water are almost equal and in the worst case, they differ by 1.5%.

Table 3
Physical properties of the water, Cu/water and Al_2O_3/water nanofluids.

Fluid	Density ($kg.m^{-3}$)	Heat capacity ($J.kg^{-1}.K^{-1}$)	Thermal conductivity (W. $m^{-1}.K^{-1}$)	Viscosity (Pa.s)
water	998	4180	0.6	0.001
Cu/ water	1013.87	4172.41	0.605	≅0.001
Al_2O_3/ water	1003.94	4173.17	0.605	≅0.001

Density ρ and heat capacity (Cp) of nanofluids can be calculated from the following equaions:

$$\rho_{nf} = \varphi\rho_{np} + (1-\varphi)\rho_{bf} \tag{1}$$

$$Cp_{nf} = \varphi Cp_{np} + (1-\varphi)Cp_{bf} \tag{2}$$

Where subscript of *nf*, *bf* and *np* related to nanofluid, base fluid and nanoparticles, respectively, and φ is the volume fraction. The Maxwell model [32], calculates the thermal conductivity of a nanofluid. This model has a good approximation and simplicity, for spherical particles in small volume fractions.

$$k_{nf} = k_{bf}\left(\frac{k_{np} + 2k_{bf} + 2\varphi(k_{np} - k_{bf})}{k_{np} + 2k_{bf} - 2\varphi(k_{np} - k_{bf})}\right) \tag{3}$$

Batchelor [33] model introduced Brownian motion effect and was developed by considering isotropic suspension of rigid and spherical nanoparticles. This model is one of the classical models of nanofluids' viscosity and is given as follows:

$$\mu_{nf} = \mu_{bf}\left(1 + 2.5\varphi + 6.5\varphi^2\right) \tag{4}$$

According to Table 3 the Reynolds numbers of outer flow in 2nd heat exchanger for water, Cu/water and Al_2O_3/water are 24.6, 24.95 and 24.73, respectively. Therefore, the results are comparable due to the same Reynolds numbers. The main reason of increasing the performance of water extraction using the nanofluids in this work is related to higher thermal inertia of the nanofluids ($\rho \times C_p$). Since the Reynolds number in 2nd heat exchanger is very low (about 24) the time of remaining the cooling fluid in heat exchanger is high and thermal inertia takes an important role in the performance increment.

2.2. Uncertainity analysis

In experimental studies, it is necessary to check the uncertainty of measurement instruments for proper analysis of output results. In this regard, the uncertainty of measurement instruments, (i.e. tool uncertainty, repetition uncertainty, and total uncertainty) are calculated as follows:

$$u_{tools} = \frac{a}{2\sqrt{3}} \tag{5}$$

$$u_{rep} = \frac{S}{\sqrt{m}} \tag{6}$$

$$u_{total} = \sqrt{{u_{tools}}^2 + {u_{rep}}^2} \tag{7}$$

Table 4
The accuracy and uncertainty of the measurement instruments.

Measurement instruments	Accuracy	Tool uncertainty	Repetition uncertainty	Total uncertainty
K-type thermocouple	0.5 °C	0.144 °C	0.214 °C	0.257 °C
Testo 605i	2%	0.577%	0.37%	0.685%
Mercury Thermometer	1 °C	0.577 °C	0.375 °C	0.685 °C
Anemometer	0.1 ±3%	0.87%	0.63%	1.07%

$$S = \sqrt{\frac{\sum_{i=1}^{m} (x_i - \bar{x})^2}{m-1}} \tag{8}$$

$$\bar{x} = \frac{\sum_{i=1}^{m} x_i}{m} \tag{9}$$

In these equations, a is the accuracy of the measuring instruments, S denotes the standard deviation, m shows the number of iterations, and x stands for the parameter. The accuracy and uncertainty of the measurement instruments are presented in Table 4.

Moreover, in order to analyze the uncertainty of different parameters, the following equations are used [34,35]:

$$R = R(x_1, x_2, \ldots, x_n) \tag{10}$$

$$\partial R = \sqrt{\left(\frac{\partial R}{\partial x_1}\right)^2 (\partial x_1)^2 + \left(\frac{\partial R}{\partial x_2}\right)^2 (\partial x_2)^2 + \ldots + \left(\frac{\partial R}{\partial x_n}\right)^2 (\partial x_n)^2} \tag{11}$$

In this equation, ∂R shows uncertainty, and R is the parameter. According to these equations, the uncertainty of the COP of the system was lower than 0.1%.

2.3. System performance analysis

To analyze the performance of the system, the refrigerant and water distillation cycles were considered as the control volumes

2.4. Refrigerant cycle

Based on this method, the energy balance for the refrigerant cycle can be presented as:

$$\sum \dot{E}_{in} = \sum \dot{E}_{out} + \sum \dot{E}_{loss} \Rightarrow \dot{E}_{comp} + \dot{E}_{eva} = \dot{E}_{con} + \dot{E}_{loss} \tag{12}$$

In this equation, $\dot{E}_{comp}$ is the input power of the compressor, $\dot{E}_{con}$ is the rate of heat transfer from the condenser to the surrounding environment, $\dot{E}_{eva}$ is the rate of heat transfer from the base fluid of the water distillation cycle to the refrigerant in the evaporator, and $\dot{E}_{loss}$ is loss energy from the system to the ambient. In this equation, the input power of the compressor can be calculated as:

$$\dot{E}_{comp} = V \bullet \mathrm{I} \tag{13}$$

In this equation, V and I are the voltage and current of the compressor. Additionally, in the evaporator, the amount of absorbed energy by the refrigerant, considered to be equal to the amount of energy that is transferred from the working fluid of the water distillation cycle to the refrigerant in the refrigeration cycle. Thus, the amount of absorbed energy by the refrigerant can be obtained as:

$$\dot{E}_{eva} = \dot{m}_{fluid} \bullet \mathrm{c}_{\mathrm{p,fluid}} \bullet \left(\mathrm{T}_{\mathrm{in,HE}} - \mathrm{T}_{\mathrm{out,HE}}\right) \tag{14}$$

Where, $\dot{m}_{fluid}$, $c_{p,\ fluid}$ are mass flow rate and heat capacity of the working fluid of the water distillation cycle. Moreover, $T_{in,\ HE}$ and $T_{out,\ HE}$ are the temperatures of the working fluid at the inlet and outlet of the heat exchanger, respectively. Also, the coefficient of performance (COP) of the refrigerant cycle can be derived as [36]:

$$COP = \frac{\dot{E}_{eva}}{\dot{E}_{comp}} \tag{15}$$

2.5. Water distillation cycle

Besides, in the water distillation cycle, the heat transfer of the working fluid to the copper spiral pipe can be written as:

$$\dot{Q}_{fluid} = \dot{m}_{fluid} \bullet \mathrm{c}_{\mathrm{p,fluid}} \bullet \left(\mathrm{T}_{\mathrm{in,ST}} - \mathrm{T}_{\mathrm{out,ST}}\right) \tag{16}$$

In this equation, $T_{in,\ ST}$ and $T_{out,\ ST}$ donates the inlet and outlet temperatures of the working fluid to the 2nd heat exchanger, respectively. Moreover, the amount of energy excluded by the airflow which leads to its temperature reduction can be calculated as:

$$\dot{Q}_{air} = \dot{m}_{air}\left[C_{p_{air}}(T_{out} - T_{in}) + w_{out}h_{go} - w_{in}h_{gi} + \dot{m}_{l,out}h_{fg}\right] \tag{17}$$

where, $\dot{m}_{l,out}$ is the mass flow rate of outlet distilled water, $T_{in,\ SP}$ and $T_{out,\ SP}$ are the air temperature at the entrance and exit of the copper spiral pipe, respectively. w_{out} and w_{in} are the specific humidity of air for outlet and inlet stream. h_{go} and h_{gi} are outlet and inlet enthalpy of saturated vapor. Moreover, $\dot{m}_{air}$, $c_{p,\ air}$ and h_{fg} are mass flow rate and heat capacity of the airflow and latent heat of water respectively.

In the copper pipe [36]:

$$\dot{m}_{air,in} = \dot{m}_{air,out} \tag{18}$$

$$\dot{m}_{v,in} = \dot{m}_{v,out} + \dot{m}_{l,out} \tag{19}$$

In the above equations, $\dot{m}_{air,in}$ and $\dot{m}_{air,out}$ are air mass flow rate at the inlet and outlet of the copper pipe. In addition $\dot{m}_{v,in}$, and $\dot{m}_{v,out}$ are vapor mass flow rate at the inlet and outlet of the copper pipe. Also, $\dot{m}_{l,out}$ is the mass flow rate of produced fresh water in the copper pipe.

The thermal efficiency of the system can be presented as:

$$\eta_{thermal} = \frac{\dot{m}_{l,out} \times h_{fg})_{T_{ave,SP}}}{input\ power\ (compressor, pump, fan)} \tag{20}$$

where, $h_{fg})_{T_{ave,\ SP}}$is phase change enthalpy at average temperature of air in the spiral pipe. In the section 5, the COP of refrigerant cycle and the total efficiency of the system in addition to the mass flow rate of the freshwater production of the system are presented.

2.6. Exergy analysis

Exergy is the maximum useful work that can be achieved from the device in the process of reaching thermodynamic equilibrium due to the second law of thermodynamics. In this system the total entered exergy is the summation of input power for compressor, pump and fan. But for computing the produced exergy, the extraction of pure water from the air moisture can be assumed as the useful output. This heat should change to work by considering Carnot efficiency. Exergy efficiency is the ratio of produced exergy to the total exergy entered the device.

$$\eta_{ex} = \frac{Ex_{product}}{Ex_{input}} = \frac{\dot{m}_{l,out} \times h_{fg})_{T_{ave,SP}} \times \left(1 - \frac{T_L}{T_H}\right)}{input\ power\ (compressor, pump, fan)} \tag{21}$$

In which T_H is considered as the inlet air temperature ($T_{in,\ SP}$) and T_L is assumed as the inlet temperature of the base fluid of distillation cycle ($T_{in,\ ST}$).

3. Cost analysis

The cost of water production is one of the most important criteria in

desalination systems. To investigate this issue, an economic analysis on the water production of the device presented above is performed and the cost of producing 1 L of water is calculated. An economic analysis on water production from solar still was done by Kabeel et al.[37].

The following relation obtains the capital recovery factor (CRF) which is a method to evaluate effective costs and identifies the success of an investment [38]:

$$CRF = \frac{i(1+i)^n}{(1+i)^n - 1} \tag{22}$$

In which i denotes the rate of lending bank interest, (18% in Iran), and n specifies the lifetime of the device, which is considered 20 years here. The first annual cost (FAC) and The first annual salvage value (ASV) of the device are as below [39]:

$$FAC = Ps \times CRF \tag{23}$$

$$ASV = S \times SSF \tag{24}$$

Where Ps is goods price and S is the salvage value of the device which is assumed 0.2Ps. SFF is sinking fund factor which is determined by the following equation.

$$SFF = \frac{CRF}{(1+i)^{\mathrm{n}}} \tag{25}$$

The annual costs of goods destruction, repair, and operation of the device can be defined as annual maintenance cost (AMC), which is equivalent to 10% of FAC [40] . The uniform annual cost (UAC) of the device is obtained as the following formula [40]:

$$UAC = FAC + AMC - ASV \tag{26}$$

In which UAC is the uniform cost of the device per year. The cost per liter of produced water which depends on the annual water production in the device can be determined by the below eq. [5]:

$$CPL = \frac{UAC}{M} \tag{27}$$

Where M is the annual water production of the device and CPL is the cost of 1 Liter of produced water by device.

To determine the energy payback time (EPBT) (the time for output energy or exergy of a device to achieve the consumed energy of constructing its materials and parts), the ratio of consumed energy of all the goods and components production used in the device (embodied energy) to output exergy or energy should be defined. The energy production factor (EPF) is a key parameter in evaluating the device performance which is equal to the total energy and exergy produced in the device to the embodied energy. These two parameters can be obtained from the following equations [41,42]:

$$EPBT_{En} = \frac{E_{in}}{(E_{en})_{out}} = \frac{1}{EPF_{En}} \tag{28}$$

$$EPBT_{Ex} = \frac{E_{in}}{(E_{ex})_{out}} = \frac{1}{EPF_{Ex}} \tag{29}$$

where E_{in} is the embodied energy which is the sum of all incorporated energy for any device production. The annual outputs of the device are determined as below [43]:

$$(E_{en})_{out} = \frac{M \times h_{fg})_{T_{ave,SP}}}{3600} \tag{30}$$

$$(E_{ex})_{out} = \frac{M \times h_{fg})_{T_{ave,SP}} \times \left(1 - \frac{T_L}{T_H}\right)}{3600} \tag{31}$$

3.1. Exergoeconomic analysis

The exergoeconomic parameter is applied in order to design a cost effective device with consideration exergy and economic analysis simultaneously. It equals to the ratio of the produced energy and exergy per year to the total annual cost (UAC) in the device. The exergoeconomic parameter based on energy and exergy is obtained by the following formula [41]:

$$R_{En} = \frac{(E_{en})_{out}}{UAC} \tag{32}$$

$$R_{Ex} = \frac{(E_{ex})_{out}}{UAC} \tag{33}$$

3.2. Environmental and exergoenvironmental cost analysis

The environmental and exergoenvironmental cost analyzed based on emission and mitigation CO_2. The carbon dioxide production and distribution are equal to 0.96 $\frac{kg}{kWh}$ without considering the device losses [44]. Due to 20% transmission and 40% distribution losses caused by the inefficient device, the CO_2 production reaches to $2\frac{kg}{kWh}$. The annual carbon dioxide emission (ACDE) and the emission of carbon dioxide during the device lifetime (LCDE) are considered as below:

$$ACDE = \frac{2 \times E_{in}}{n} \tag{34}$$

$$LCDE = 2 \times E_{in} \tag{35}$$

The annual CO_2 mitigation rate in a device based on energy and exergy can be calculated as follows [45]:

$$\phi_{en,CO_2} = \frac{2\left((E_{en})_{out} \times n - E_{in}\right)}{1000} \tag{36}$$

$$\phi_{ex,CO_2} = \frac{2\left((E_{ex})_{out} \times n - E_{in}\right)}{1000} \tag{37}$$

Where $\phi_{en,\ CO2}$ and $\phi_{ex,\ CO2}$are the environmental and exergoenvironmental parameters, respectively. The price of the CO_2 mitigation based on energy and exergy can be calculated in the following relation, respectively [46]:

$$Z_{en,CO_2} = X_{CO_2} \times \phi_{en,CO_2} \tag{38}$$

$$Z_{ex,CO_2} = X_{CO_2} \times \phi_{ex,CO_2} \tag{39}$$

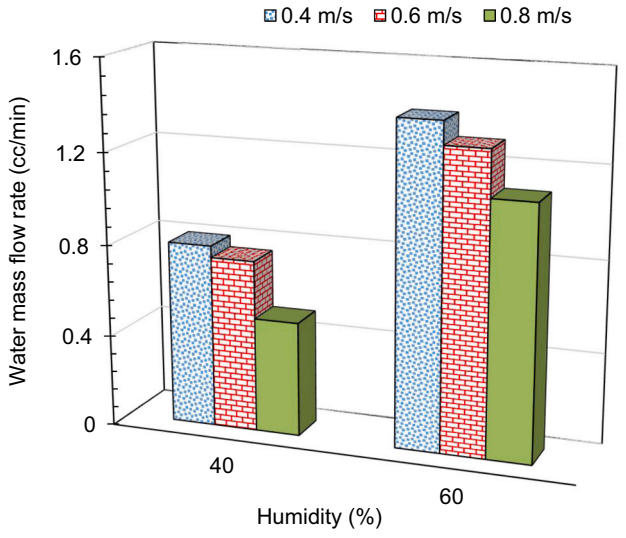

Fig. 2. The amount of produced water by the system at different air temperatures and ambient humidity using water as based fluid of distillation cycle.

Table 5
Test condition of the pure water as the base fluid of the distillation cycle for 40% humidity.

Parameter	Air velocity of 0.4 m/s	Air velocity of 0.6 m/s	Air velocity of 0.8 m/s
Inlet water temperature (°C)	10	10	10
Outlet water temperature (°C)	13	13	12
Inlet air temperature (°C)	32	32	26
Outlet air temperature (dew point temperature) (°C)	18.6	18.2	12.1
Ambient temperature (°C)	25.6	25.6	24.8
Rate of produced water (cc/min)	0.8	0.75	0.5

Table 6
The output results of the examination of the designed system at different humidity using pure water as the base fluid for 0.8 air velocity.

Parameter	Ambient humidity of 40%	Ambient humidity of 60%
Inlet water temperature (°C)	10	10
Outlet water temperature (°C)	12	14
Inlet air temperature (°C)	26	31
Outlet air temperature (dew point temperature) (°C)	12.1	22.3
Air velocity (m/s)	0.8	0.8
Ambient temperature (°C)	24.8	28.3
Rate of produced water (cc/min)	0.5	1.1

In which $Z_{en,\ CO2}$ and $Z_{ex,\ CO2}$ are the price of the CO_2 mitigation based on energy and exergy respectively and X_{CO2} indicates the international price of carbon, which is considered $14.5 per ton of CO_2 [42].

4. Results

In this study, the performance of a coupled system consisting of refrigerant and water distillation cycles was investigated. For a comprehensive investigation of the system performance, the effect of air velocity and ambient humidity was addressed. Moreover, the effect of dispersion of Cu and Al_2O_3 nanoparticles in the base fluid of the water distillation cycle was also investigated.

4.1. Performance analysis

The results related to the pure water working fluid are presented in Fig. 2 at different air velocities. The amount of produced water by the system at different air velocities (0.4, 0.6, and 0.8 m/s) and ambient humidity values (40% and 60%) are also presented. The results of the system with pure water base fluid are illustrated in Table 5 for the humidity level of 40%.

According to Fig. 2, variations in both air velocity and ambient humidity drastically affected the system performance. As presented, the inlet temperature of the water fluid to the 2nd heat exchanger was 10 °C. Moreover, the ambient humidity was determined to be about 40% and 60%. According to the results, in the ambient humidity of 40%, a reduction in the air velocity from 0.8 m/ to 0.4 m/s enhanced the amount of produced water from 0.5 to 0.8 cc/min. In fact, by reducing the air velocity, the air remains longer in the copper spiral pipe which leads to its more temperature decline. At a higher reduction in the air temperature, more amount of air moisture will transfer from the gas to the liquid phase.

Moreover, it is found that increasing the ambient humidity has a huge effect on the performance of the system. Based on Fig. 2, a rise in the ambient humidity from 40% to 60% enhanced the water production by around 75% and 120% for the system with air velocities of 0.4 m/s and 0.8 m/s, respectively. The results obtained from the system with the

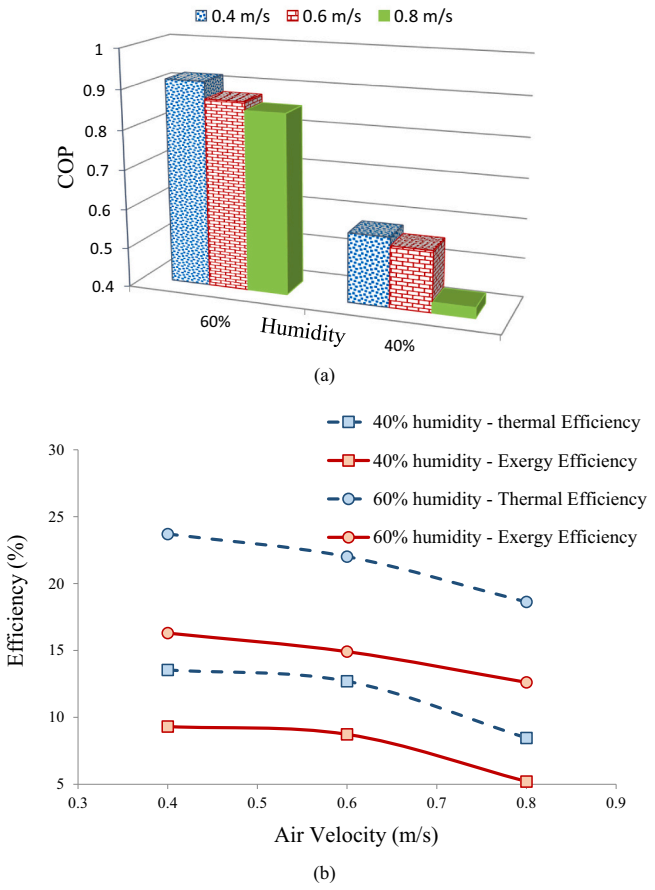

Fig. 3. The amount of (a) COP, and (b) Thermal and exergy efficiencies of the system at various air velocities and ambient humidity using water as based fluid of distillation cycle.

air velocity of 0.8 m/s and ambient humidity of 40% and 60% are presented in Table 6. Furthermore, the COP and total efficiency of the system are depicted in Fig. 3 (a) and (b), respectively.

As presented in Table 6 and Fig. 3, by increasing the ambient humidity from 40% to 60%, the amount of freshwater was enhanced from 0.5 to 1.1 cc/min, which shows the high effect of ambient humidity on freshwater production by the system. Also, it is observed that the outlet temperature of the water fluid from the 2nd heat exchanger in the ambient humidity of 60% was much higher than that of 40%. At higher ambient humidity, more amount of energy will transfer from the working fluid of the water distillation cycle to the airflow due to the increment in the production of the liquid water by the system. Thus, it is expected that raising the humidity of the surrounding environment causes a higher outlet temperature of working fluid from the 2nd heat exchanger.

Additionally, according to Fig. 3, the COP of the refrigerant cycle at ambient humidity of 40% and air velocities 0f 0.4, 0.6, and 0.8 m/s were 0.57, 0.55, and 0.42, respectively. Moreover, it was found that these values for the ambient humidity of 60% are 0.92, 0.87, and 0.85, respectively. It should be noted that due to the fact that the device consists of two separate cycles, the rate of heat loss is high. Therefor the small COP is obtained for this system. However, since in the present work, the aim is to investigate the effect of nanofluid on the extraction of air humidity, so it is not important to obtain a low COP. However, by combining two separate cycles in this device in future research works, the value of the COP can be increased.

According to the obtained results, at lower humidities, a rise in the air velocity from 0.4 to 0.6 m/s did not considerably affect the COP of

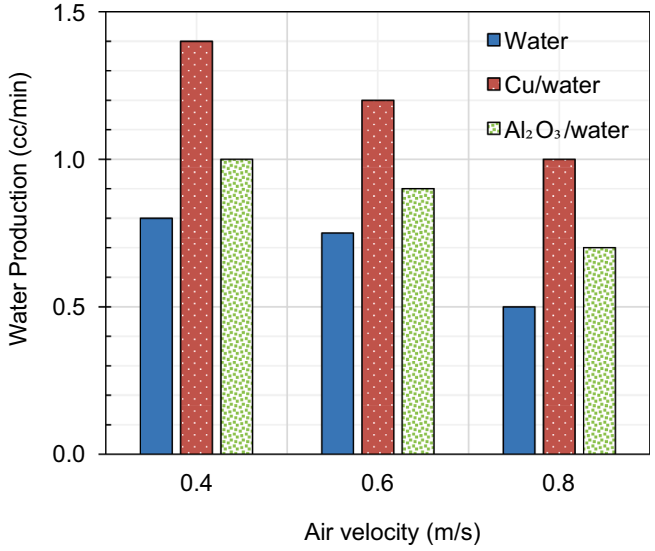

(a)

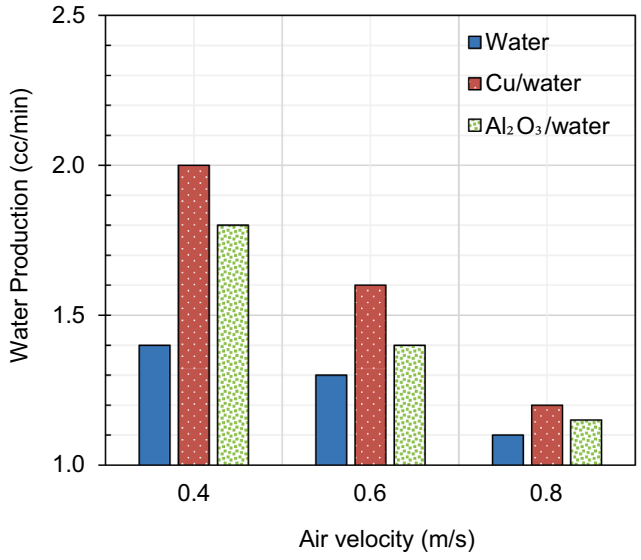

(b)

Fig. 4. The mass flow rate of produced freshwater by the system at different working conditions a) 40% humidity b) 60% humidity.

the system, while raising the air velocity from 0.6 to 0.8 m/s remarkably declined the COP of the system. Elevation of the air velocity led to lower heat transfer from the copper pipe to the airflow due to the shorter time that air remained in the copper pipe. It was shown that an increment in the ambient humidity from 40% to 60% could enhance the COP of the system from around 0.5 to 0.9.

Fig. 3 (b) presents the amount of 1st and 2nd Law efficiencies of the system at ambient humidity of 40% and 60% and air velocities of 0.4, 0.6, and 0.8 m/s. Based on the obtained data, an increase in the air velocity reduced these efficiencies of the system due to a lower amount of freshwater production. Moreover, higher humidity led to higher efficiencies due to higher water extraction from the air moisture. So that a 20% increase in humidity caused 89% and 96% increment in thermal and exergy efficiencies of the system, respectively.

In Fig. 4 (a) and (b), the amount of produced freshwater by the system is presented by using various working fluids at the ambient humidity of 40% and 60%. According to this figure, increasing the air

Table 7
The output results of the examination of the designed system at different air velocities with using Cu/water nanofluid as the working fluid of the system for 40% humidity.

Parameter	Air velocity of 0.4 m/s	Air velocity of 0.6 m/s	Air velocity of 0.8 m/s
Inlet nanofluid temperature (°C)	11	11	10
Outlet nanofluid temperature (°C)	14	14	13
Inlet air temperature (°C)	30	30	30
Outlet air temperature (dew point temperature) (°C)	14.9	16.4	15.7
Ambient temperature (°C)	25.4	25.7	23.1
Rate of produced water (cc/min)	1.4	1.2	1.0

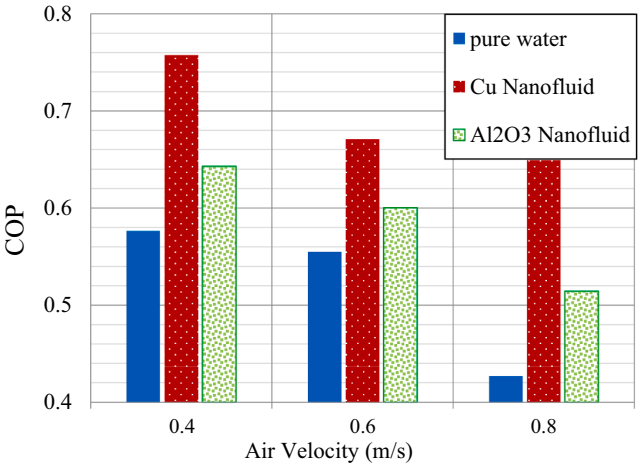

(a)

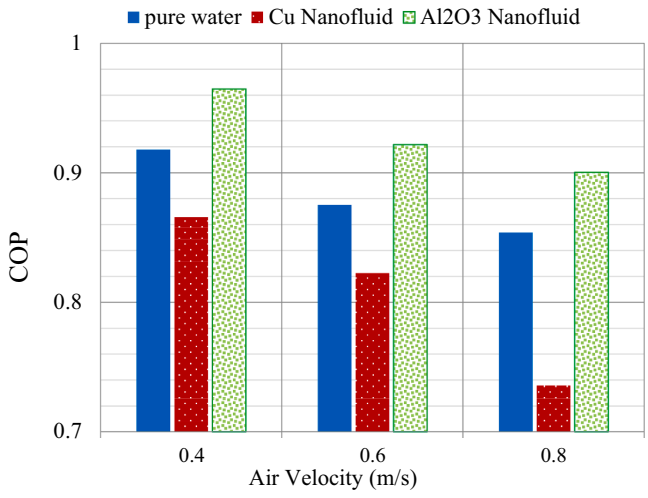

(b)

Fig. 5. The amount of COP of the system at different air velocity and different working fluid of distillation cycle a) 40% humidity b) 60% humidity.

velocity from 0.4 ms to 0.8 m/s declined the amount of produced freshwater by about 21%, 40%, and 33% for the working fluids of pure water, Cu/water, and Al_2O_3/water, respectively. The highest and lowest sensitivity to the air velocity was observed in the Cu/water nanofluid and pure water, respectively. Additionally, the amount of produced freshwater at the ambient humidity of 40% and air velocity of 0.4 m/s

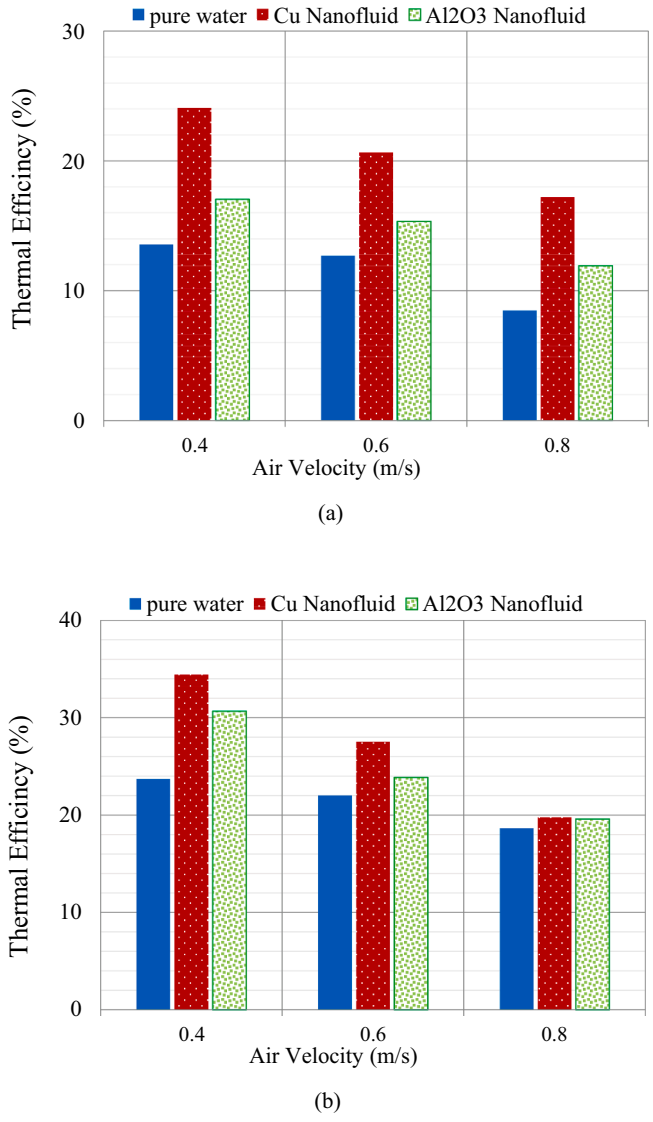

Fig. 6. The amount of thermal efficiency of the system at different air velocity and different working fluid of distillation cycle a) 40% humidity b) 60% humidity.

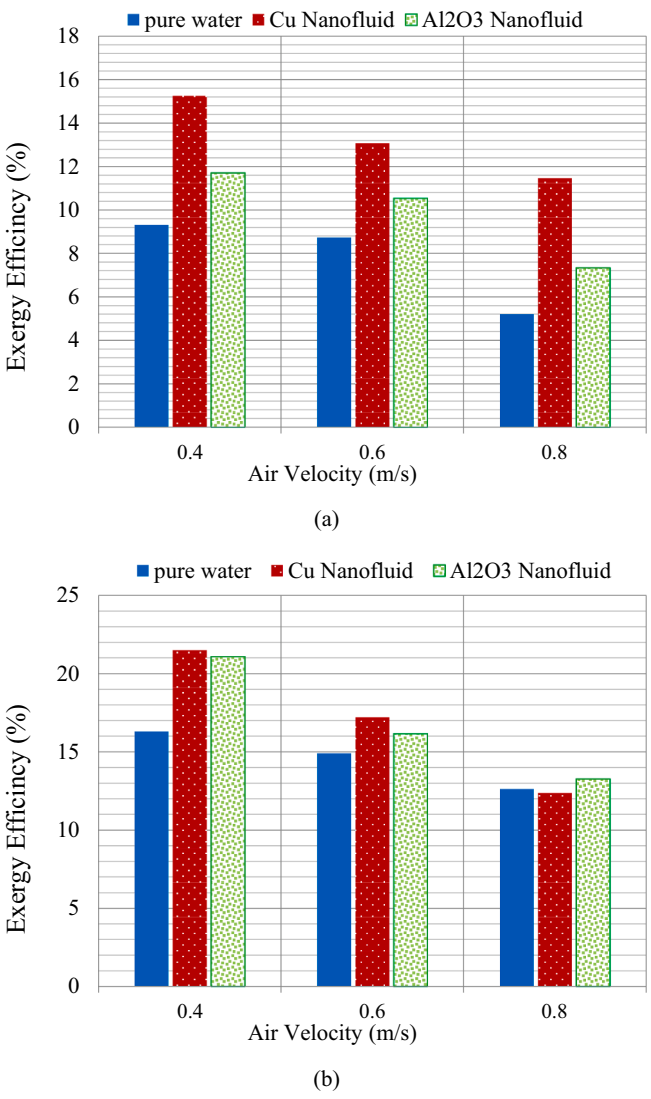

Fig. 7. The amount of Exergy efficiency of the system at different air velocity and different working fluid of distillation cycle a) 40% humidity b) 60% humidity.

was 0.8, 1.0, and 1.4 cc/min for the working fluids of pure water, Cu/water, and Al_2O_3/water, respectively. It was also found that in the ambient humidity of 60% and air velocity of the 0.4 m/s, the amount of freshwater production by using Cu/water and Al_2O_3/water was approximately 43% and 29% higher than that of pure water working fluid, respectively.

According to Fig. 4, the Cu/water nanofluid-based system showed the best performance. The high thermal conductivity of the Cu nanoparticles can enhance the heat transfer from the working fluid to the copper pipe, giving rise to higher freshwater production. When nanofluids are used, the water production is increased, but the pump work will be increased too due to enhancement in fluid viscosity. But, since in this study, the mass fraction of NPs used in nanofluids is low (0.2%), so it will not have much effect on fluid viscosity and pump power consumption. However, in case of using nanofluids with higher concentrations, the effect of pump power consumption must be considered in the observations. The detailed results of the system using Cu/water nanofluid as the working fluid are presented in Table 7.

The amount of COP is presented in Fig. 5 for the system using pure water, Cu/water, and Al_2O_3/water at different air velocities and humidity levels. Dispersion of Cu and Al_2O_3 nanoparticles in the base fluid (pure water) will enhance the thermal properties of the working fluid increases due to the higher thermal conductivity of the nanoparticles in comparison to the base fluid. This will result in higher thermal absorption from the refrigerant cycle by the working fluid in the heat exchanger.

Based on the reported data, at 40% humidity, the COP of the system using Cu/water nanofluid at the air velocities of 0.4, 0.6, and 0.8 m/s were 31%, 22%, and 51% higher than the one using pure water, respectively. Moreover, the performance of the system using Cu/water nanofluid was higher than the one using Al_2O_3/water. At 60% humidity, however, the COP of the system using Cu/water nanofluid was the lowest; while the Al_2O_3 nanofluid was the best one in terms of COP.

According to Fig. 6, for 40% humidity, the thermal efficiency of the system using Cu/water nanofluid was around 77.8%, 62.5%, and 102%

Table 8
Cost of fabricated device.

Device Components	Cost ($)	Salvage value ($)
Refrigration Cycle	128/5	25/7
Structure	17/1	3/42
1st heat exchanger	17/5	3/5
2nd heat exchanger	57/1	11/42
Linear pump	25	5
Exhaust fan	23	4/6
Electrical equipments	33/5	6/7
Sensors and Measurment instruments	20/3	4/06
Pipes and fittings	18/3	3/66
Nanofluid	32	6/4
Total Cost (water base)	340/3	68/06
Total Cost (nanofluid base)	372/3	74/46

higher than the one employing pure water, respectively. Further, the efficiency of the system using Al_2O_3/water as the working fluid of the system was approximately 25.6%, 20.7%, and 41%, higher than the one using pure water at different air velocities of 0.4, 0.6, and 0.8 m/s, respectively. The reason for the better performance of the system using Cu/water could be assigned to the higher thermal conductivity of the Cu compared to Al_2O_3. Fig. 6(b) shows that at higher air velocities and humidities, the use of nanofluids has a minor effect on system performance. At this humidity, the improvement of system performance for lower velocities (0.4 m/s and 0.6 m/s) due to the use of nanofluids was lower than that of 40% humidity.

Fig. 7 indicates the exergy efficiency of the systems using different working fluid and at different air velocities for the ambient humidity of 40% and 60%. At high humidity and air velocity, Al_2O_3 nanofluid exhibited the best exergy efficiency as compared with other working fluids. In general, at high moisture content, the exergy efficiencies of the two nanofluids are close to each other.

4.2. Economic analysis

After a comprehensive review of the economic analysis in Section 4, the related results are investigated in this section. The fabrication cost of the device and its salvage value were estimated according to Table 8. The results show that the fabrication cost of the nanofluid-based devices was about 10% higher than a water-based setup.

The cost of water production for water-based and nanofluid-based devices is presented in Table 9. This table presents the best water production rate for two cases (i.e.1.4 cc/min for water-based and 2 cc/min for Cu nanofluid-base device). The related conditions involved 0.4 m/s air velocity and 60% environment humidity. A comparison of these two cases indicated a 42% enhancement in the annual water production upon using Cu nanofluid instead of water as the working fluid in the distillation cycle. As observed, the water production cost in the nanofluid-based device was 32% lower than the water-based set-up due to the higher annual water production.

Table 10 presents the details of the embodied energy to produce different materials and components used in the device. The embodied energy of the water-based and the nanofluid-based devices are approximately similar, and their difference is just in the embodied energy for nanoparticle production which is about 0.3% of the total embodied energy of the device. The embodied energy of Cu nanoparticle production has been obtained from ref. [47].

Table 11 indicates the energy payback time (EPBT) and the energy production factor (EPF) based on exergy and energy which requires estimating the annual output energy and exergy in kWh for the water-based and nanofluid-based devices. The results indicate that the EPBT of the water-based devices was more than the nanofluid-based ones, which can be due to the lower annual output energy and exergy of the water-based devices compared to the nanofluid-based one (considering the same embodied energy). Also, it can be observed that the EPF of the nanofluid-base device was higher than the water-based one, which is due to higher annual output energy and exergy.

Table 12 shows the exergoeconomic, environmental, enviroeconomic, exergoenvironmental, and exergoenviroeconomic parameters of the device. As observed, the exergoeconomic parameters based on energy and exergy (the ratio of the annual produced energy and exergy to the total annual cost) are enhanced by 30% and 19.2% in the nanofluid-based systems, respectively, as compared with the water-based one. This can be attributed to the higher annual outputs. The annual energy and exergy outputs of the nanofluid-based systems were increased by 42% and 29.7% comparing with the water-based set-up, respectively. The CO_2 mitigation in the nanofluid-based system was approximately 42.5% higher than the water-based device, due to the higher annual energy output during lifetime considering the embodied energy. Moreover, environmental, enviroeconomic, exergoenvironmental and exergoenviroeconomic parameters of the nanofluid-based systems are higher than the water-based set-up.

Table 10
Embodied energy of different component of the device.

Device Components	Mass of components (kg)	Portion of materials	Energy density (Mj/kg)	Embodied energy (kWh)
Refrigeration cycle	7.98	82% steel	32	58
		15% copper	70.6	23.41
		3% PVC	70	4.64
Structure	13.2	96% Iron	25	87.75
		4% polyester	53.7	78.54
1st heat exchanger	0.95	32% PVC	70	5.89
		42% copper	70.6	7.8
		24% brass	62	3.92
		2% polyester	53.7	0.28
2nd heat exchanger	4.25	44% PVC	70	36.26
		11% plaxiglass	102	13.21
		5% Brass	62	3.65
		40% Copper	70.6	33.24
Linear pump	2.8	46% cast Iron	13.5	4.82
		34% copper	70.6	18.62
		4% Iron	25	0.78
		16% polyester	53.7	6.67
Exhaust fan	1.8	55% Iron	25	6.86
		27% Aluminum	191	25.71
		18% Copper	70.6	6.34
Electrical equipments	2.3	65% Iron	25	10.35
		21% polyester	53.7	7.18
		14% Copper	70.6	6.3
Pipes and fittings	2.8	8% Polypropylene	95.4	5.92
		4% PVC	70	2.17
		11% brass	62	5.29
		71% Steel	32	17.62
Nanofluid	7.5	0.2% Cu nanoparticle	[47] 350	1.45
		99.8% water	0.01	0.021
Total				482.695

Table 9
Cost analysis for water_based and nanofluid-based device.

Type	n	i	CRF	FAC ($/year)	SSF	S ($)	ASV ($/year)	AMC ($/year)	UAC ($/year)	M (L/year)	CPL ($/L)
water_based	20	0.18	0.187	63.57	0.007	68	0.46	6.36	69.47	735.84	0.095
nanofluid-based	20	0.18	0.187	69.62	0.007	74.5	0.51	6.96	76.1	1051.2	0.072

Table 11
Energy payback time and Energy production factor of the device.

Type	M (L/year)	Embodied energy (kWh)	$(E_{en})_{out}$ (kWh/year)	$(E_{ex})_{out}$ (kWh/year)	$EPBT_{en}$ (year)	$EPBT_{ex}$ (year)	EPF_{en}	EPF_{ex}
water_based	735.84	481.545	501.5	36.2	0.96	13.31	1.04	0.075
nanofluid-based	1051.2	482.695	716.4	46.98	0.67	10.27	1.48	0.097

Table 12
Exergoeconomic, environmental and enviroeconomic parameters for the device.

Parameter	Water_based	Nanofluid_based
Life time (years)	20	20
Embodied Energy (kWh)	481.545	482.695
Annual Energy output (kWh/year)	501.5	716.4
Annual Exergy output (kWh/year)	36.2	46.98
the ratio of the annual produced energy to the total annual cost (kWh/$)	7.22	9.41
the ratio of the annual produced exergy to the total annual cost (kWh/$)	0.52	0.62
Annual Carbon dioxide emission	48.15	48.26
Lifetime Carbon dioxide emission (kg)	963.1	965.4
Lifetime Carbon dioxid mitigation (ton)	20.1	28.65
Environmental parameter (ton Co2)	19.1	27.7
Enviroeconomic parameter ($)	276.9	401.53
Exergoenvironmental parameter (ton Co2)	0.48	0.91
Exergoenviroeconomic parameter ($)	7.02	13.25

5. Conclusion

The performance of a coupled system consisting of a refrigerant cycle and a water distillation cycle was comprehensively investigated. In the present research, various parameters including mass flow rate of the produced freshwater, COP, and total efficiency of the system were studied under various working conditions. To study the effect of ambient humidity, the system was examined at ambient humidity of 40% and 60%. Moreover, the effect of inlet air velocity on the copper spiral pipe was explored by varying air velocity from 0.4 m/s to 0.8 m/s. Additionally, the effect of Cu and Al_2O_3 nanoparticles dispersion in the base fluid of the water distillation cycle on the performance of the system was analyzed. The most remarkable findings of the present paper can be summarized as:

- Increasing air velocity reduced the amount of freshwater production of the system, while an increment in the ambient humidity significantly enhanced the system performance.
- For the pure water-based system, by increasing the ambient humidity from 40% to 60%, the COP of the system grew from around 0.5 to 0.9.
- By adding Cu nanoparticles to the pure water, the amount of freshwater production of the system increased from 0.8 to 1.4 cc/min, respectively, at the air velocity of 0.4 m/s and ambient humidity of 60%.
- Using the Cu/water nanofluid-based system at 40% humidity, 31%, 22%, and 51% improvement was detected in the total efficiency of the system at the air velocities of 0.4, 0.6, and 0.8 m/s, respectively when compared with the pure water-based system.
- The Cu/water nanofluid-based system exhibited the highest performance among the studied cases due to its high thermal conductivity of the Cu nanoparticles.
- For higher air velocities and humidity, no significant difference was observed in total efficiency upon using nanofluids when compared with pure water.
- According to the economic analysis, the application of Cu nanofluid instead of water as the working fluid of the distillation cycle led to a 42% increase in the annual water production resulting in a 32% reduction of the water production cost in the nanofluid-based system.
- The CO_2 mitigation in the nanofluid-based system was approximately 42.5% higher than the water-based device.
- The environmental, enviroeconomic, exergoenvironmental, and exergoenviroeconomic parameters of the nanofluid-based devices were higher than the water-based systems.

Credit author statement

Masoud Kaveh; Investigation, experimental design and manufacturing, Data Gathering.

Writing - Original Draft, Performing the experimental procedures.

Ali Heydari: Methodology, Writing - Review & Editing, Supervision, Conceptualization,

Investigation.

Nader Rahbar: Writing - Review & Editing, Supervision, Data Curation,

Abdollah KhalesiDoost: Review & Editing, Supervision,

All authors reviewed the final manuscript.

Declaration of competing interest

The authors whose names are listed immediately below certify that they have NO affiliations with or involvement in any organization or entity with any financial interest (such as honoraria; educational grants; participation in speakers' bureaus; membership, employment, consultancies, stock ownership, or other equity interest; and expert testimony or patent-licensing arrangements), or non-financial interest (such as personal or professional relationships, affiliations, knowledge or beliefs) in the subject matter or materials discussed in this manuscript.

References

[1] B.S.U.N.E. Programme, Essential Concepts of Global Environmental Governance, 2014, p. 229.
[2] M. Mohamed, G. William, M. Fatouh, Solar energy utilization in water production from humid air, Sol. Energy 148 (2017) 98–109.
[3] A. Nafey, et al., Solar desalination using humidification–dehumidification processes. Part II. An experimental investigation, Energy Convers. Manag. 45 (7–8) (2004) 1263–1277.
[4] T. Rajaseenivasan, K. Srithar, Potential of a dual purpose solar collector on humidification dehumidification desalination system, Desalination 404 (2017) 35–40.
[5] A. Heydari, N. Rahbar, Energy and life cost analysis of a wet wall solar still with various pump working conditions, Environ. Prog. Sustain. Energy 36 (2) (2017) 532–538.
[6] H. Garg, R.S. Adhikari, R. Kumar, Experimental design and computer simulation of multi-effect humidification (MEH)-dehumidification solar distillation, Desalination 153 (1–3) (2003) 81–86.
[7] G. Al-Enezi, H. Ettouney, N. Fawzy, Low temperature humidification dehumidification desalination process, Energy Convers. Manag. 47 (4) (2006) 470–484.
[8] N.I. Ibrahim, F.A. Al-Sulaiman, R. Saidur, Performance assessment of water production from solar cooling system in humid climate, Energy Convers. Manag. 127 (2016) 647–655.
[9] A. Fouda, S. Nada, H. Elattar, An integrated A/C and HDH water desalination system assisted by solar energy: transient analysis and economical study, Appl. Therm. Eng. 108 (2016) 1320–1335.
[10] F. Jabari, et al., A solar dish Stirling engine combined humidification-dehumidification desalination cycle for cleaner production of cool, pure water, and power in hot and humid regions, Sust. Energy Technol. Assess. 37 (2020), 100642.
[11] R. Ghasemiasl, et al., Exergetic and economic optimization of a solar-based cogeneration system applicable for desalination and power production, J. Therm. Anal. Calorim. (2020) 1–11.
[12] A. Mohamed, A.G. Shahdy, M.S. Ahmed, Investigation on solar humidification dehumidification water desalination system using a closed-air cycle, Appl. Therm. Eng. 188 (2021), 116621.

[13] E. Chantoiseau, et al., Heat-pump dehumidifier as an efficient device to prevent condensation in horticultural greenhouses, Biosyst. Eng. 142 (2016) 27–41.
[14] M. Faegh, M.B. Shafii, Performance evaluation of a novel compact humidification-dehumidification desalination system coupled with a heat pump for design and off-design conditions, Energy Convers. Manag. 194 (2019) 160–172.
[15] D. Lawal, et al., Humidification-dehumidification desalination system operated by a heat pump, Energy Convers. Manag. 161 (2018) 128–140.
[16] B. Omidi, et al., Combination of a solar collector and thermoelectric cooling modules in a humidification–dehumidification desalination system-experimental investigation with energy, exergy, exergoeconomic and environmental analysis, Energy Convers. Manag. 225 (2020), 113440.
[17] H. Rostamzadeh, et al., Feasibility investigation of a humidification-dehumidification (HDH) desalination system with thermoelectric generator operated by a salinity-gradient solar pond, Desalination 462 (2019) 1–18.
[18] Y. Cao, et al., Thermo-economic evaluation of a combined Kalina cycle and humidification-dehumidification (HDH) desalination system integrated with thermoelectric generator and solar pond, Int. J. Heat Mass Transf. 168 (2021), 120844.
[19] H. Al-Madhhachi, G. Min, Key factors affecting the water production in a thermoelectric distillation system, Energy Convers. Manag. 165 (2018) 459–464.
[20] B.A. Habeebullah, Potential use of evaporator coils for water extraction in hot and humid areas, Desalination 237 (1–3) (2009) 330–345.
[21] S. Zolfagharkhani, M. Zamen, M.M. Shahmardan, Thermodynamic analysis and evaluation of a gas compression refrigeration cycle for fresh water production from atmospheric air, Energy Convers. Manag. 170 (2018) 97–107.
[22] M. Sardarabadi, M. Passandideh-Fard, S.Z. Heris, Experimental investigation of the effects of silica/water nanofluid on PV/T (photovoltaic thermal units), Energy 66 (2014) 264–272.
[23] A. Hassan, et al., Thermal management and uniform temperature regulation of photovoltaic modules using hybrid phase change materials-nanofluids system, Renew. Energy 145 (2020) 282–293.
[24] J. Koo, C. Kleinstreuer, Impact analysis of nanoparticle motion mechanisms on the thermal conductivity of nanofluids, Int. Communicat. Heat Mass Transfer 32 (9) (2005) 1111–1118.
[25] A. Abdelrazik, F. Al-Sulaiman, R. Saidur, Numerical investigation of the effects of the nano-enhanced phase change materials on the thermal and electrical performance of hybrid PV/thermal systems, Energy Convers. Manag. 205 (2020), 112449.
[26] A. Salari, et al., An updated review of the performance of nanofluid-based photovoltaic thermal systems from energy, exergy, economic, and environmental (4E) approaches, J. Clean. Prod. 282 (1) (2020), 124318.
[27] K. Garg, et al., Parametric study of the energy efficiency of the HDH desalination unit integrated with nanofluid-based solar collector, J. Therm. Anal. Calorim. 135 (2) (2019) 1465–1478.
[28] M.R. Salimpour, A. Shahmoradi, D. Khoeini, Experimental study of condensation heat transfer of R-404A in helically coiled tubes, Int. J. Refrig. 74 (2017) 584–591.
[29] N. Essalhi, et al., Design of helical coil condenser of small-capacity Water/Lithium Bromide absorption cooling machine, Int. J. Hydrog. Energy **42** (13) (2017) 8888–8897.
[30] G. Liu, et al., Experimental study on heat transfer characteristics of a condenser in the presence of air, Appl. Therm. Eng. 120 (2017) 170–178.
[31] A.K. Solanki, R. Kumar, Condensation of R-134a inside dimpled helically coiled tube-in-shell type heat exchanger, Appl. Therm. Eng. 129 (2018) 535–548.
[32] W. Yu, et al., Review and comparison of nanofluid thermal conductivity and heat transfer enhancements, Heat Transfer Eng. 29 (5) (2008) 432–460.
[33] G.K. Batchelor, The effect of Brownian motion on the bulk stress in a suspension of spherical particles, J. Fluid Mech. 83 (1) (1977) 97–117.
[34] S.K. Verma, A.K. Tiwari, Progress of nanofluid application in solar collectors: a review, Energy Convers. Manag. 100 (2015) 324–346.
[35] M. Ebrahimi-Dehshali, S.Z. Najm-Barzanji, A. Hakkaki-Fard, Pool boiling heat transfer enhancement by twisted-tape fins, Appl. Therm. Eng. 135 (2018) 170–177.
[36] C. Borgnakke, R.E. Sonntag, Fundamentals of Thermodynamics: Part 1, John Wiley & Sons, Inc, 2009.
[37] A.E. Kabeel, A.M. Hamed, S.A. El-Agouz, Cost analysis of different solar still configurations, Energy 35 (7) (2010) 2901–2908.
[38] S. Shoeibi, et al., Application of simultaneous thermoelectric cooling and heating to improve the performance of a solar still: an experimental study and exergy analysis, Appl. Energy 263 (2020), 114581.
[39] A. Agrawal, R.S. Rana, Theoretical and experimental performance evaluation of single-slope single-basin solar still with multiple V-shaped floating wicks, Heliyon 5 (4) (2019), e01525.
[40] P. Dumka, A. Jain, D.R. Mishra, Energy, exergy, and economic analysis of single slope conventional solar still augmented with an ultrasonic fogger and a cotton cloth, J. Ener. Stor. 30 (2020), 101541.
[41] M.S. Yousef, H. Hassan, Assessment of different passive solar stills via exergoeconomic, exergoenvironmental, and exergoenviroeconomic approaches: a comparative study, Sol. Energy 182 (2019) 316–331.
[42] S.M. Parsa, et al., Energy-matrices, exergy, economic, environmental, exergoeconomic, enviroeconomic, and heat transfer (6E/HT) analysis of two passive/active solar still water desalination nearly 4000m: altitude concept, J. Clean. Prod. 261 (2020), 121243.
[43] T. Rajaseenivasan, K. Srithar, Performance investigation on solar still with circular and square fins in basin with CO2 mitigation and economic analysis, Desalination 380 (2016) 66–74.
[44] B.K. Sovacool, Valuing the greenhouse gas emissions from nuclear power: a critical survey, Energy Policy 36 (8) (2008) 2950–2963.
[45] S. Shoeibi, et al., Energy Matrices, Exergoeconomic and Enviroeconomic Analysis of Air-Cooled and Water-Cooled Solar Still: Experimental Investigation and Numerical Simulation 171, 2021, pp. 227–244.
[46] A.R.A. Elbar, M.S. Yousef, H. Hassan, Energy, exergy, exergoeconomic and enviroeconomic (4E) evaluation of a new integration of solar still with photovoltaic panel, J. Clean. Prod. 233 (2019) 665–680.
[47] L.M. Gilbertson, et al., Guiding the design space for nanotechnology to advance sustainable crop production, Nat. Nanotechnol. 15 (9) (2020) 801–810.